



Full Text View

[Volume 29, Issue 8 \(August 1999\)](#)

Journal of Physical Oceanography

Article: pp. 1881–1891 | [Abstract](#) | [PDF \(173K\)](#)

The Effect of Continental Slope on Buoyancy-Driven Circulation

Lixin Wu and Zhengyu Liu

Department of Atmospheric and Oceanic Science, University of Wisconsin—Madison, Madison, Wisconsin

Harley E. Hurlburt

Naval Research Laboratory, Stennis Space Center, Mississippi

(Manuscript received October 10, 1997, in final form September 21, 1998)

DOI: 10.1175/1520-0485(1999)029<1881:TEOCSO>2.0.CO;2

ABSTRACT

The effect of continental slope on buoyancy-driven circulation has been studied using a two-layer quasigeostrophic model. In the model, buoyancy flux is incorporated as interfacial mass flux, which consists of narrow intense detrainment in the north and broad entrainment in the south. The model explicitly shows that, in the presence of the continental slope, a small amount of buoyancy flux can drive a strong barotropic flow. This flow develops because the beta effect of bottom topography either reduces or deflects the buoyancy-driven deep flow so that it cannot compensate its overlying counterflow, thus generating a net transport. As a result, in a double gyre circulation with a western continental slope, a small amount of detrainment/entrainment water mass can substantially enhance the transport of the western boundary current through southwestern deflection of the deep subpolar circulation. For example, with a reasonable western continental slope, a 10 Sv ($\text{Sv} \equiv 10^6 \text{ m}^3 \text{ s}^{-1}$) detrainment mass flux can increase the transport of the western boundary current from 40 Sv of the wind-driven transport to 148 Sv. Relevance to the North Atlantic is then discussed.

1. Introduction

Observations have shown that transport of the Gulf Stream in the North Atlantic is much stronger than that of the Kuroshio Current in the North Pacific ([Joyce and Schmitz 1988](#); [Schmitz and McCartney 1993](#)). This significant difference cannot be generated by the wind stress over these two basins alone. In fact, due to the effect of the basin zonal dimension, the wind-driven transport in the North Pacific subtropic gyre can be much stronger than that

Table of Contents:

- [Introduction](#)
- [Model formulation](#)
- [Mechanism of the joint](#)
- [Sensitivity study](#)
- [Summary and discussion](#)
- [REFERENCES](#)
- [TABLES](#)
- [FIGURES](#)

Options:

- [Create Reference](#)
- [Email this Article](#)
- [Add to MyArchive](#)
- [Search AMS Glossary](#)

Search CrossRef for:

- [Articles Citing This Article](#)

Search Google Scholar for:

- [Lixin Wu](#)
- [Zhengyu Liu](#)
- [Harley E. Hurlburt](#)

in the North Atlantic subtropic gyre (Hurlburt et al. 1996). One possible explanation in transports is the strong buoyancy flux in the North Atlantic, which in turn drives a meridional overturning cell. In the presence of bottom topography, this baroclinic process can have a tremendous impact on the barotropic flow. This effect is clearly shown in a prognostic OGCM study with bottom topography and buoyancy forcing included in a wind-driven ocean model (Holland 1973), where the western boundary current has transport much larger than that predicted from the wind-stress distribution, even in the absence of the nonlinear advection. In the context of vorticity dynamics, this joint effect of baroclicity and bottom relief (JEBAR), represented in the diagnostic vorticity equation formed from the depth-averaged momentum equations, involves a Jacobian of the potential energy anomaly and depth (Huthnance 1984; Sakamoto and Yamagata 1996). Physically, it represents a correction to the topography vortex stretching associated with the depth-averaged flow, or the difference between the bottom pressure torque and a corresponding torque associated with the depth-averaged pressure (Mertz and Wright 1992).


Since the pioneering work of Sarkisyan and Ivaov (1971), the JEBAR effect on oceanic circulation has been diagnosed extensively in calculations of the large-scale ocean circulation. For example, Mellor et al. (1982) find this driving mechanism to be important in a diagnostic calculation of the Atlantic circulation. Greatbatch et al. (1991) showed that the bottom-pressure torque component of JEBAR was fundamental for the formation and strength of their model Gulf Stream. Myers et al. (1996) have also found this effect of the bottom pressure torque to be crucial in the transport and separation of the Gulf Stream.

However, a diagnostic study, which usually uses the observed density field, cannot conclude whether the bottom pressure torque drives the Gulf Stream or the Gulf Stream sets up the necessary density gradient to produce the observed bottom pressure torque (Myers et al. 1996). It is also hard to deduce the underlying physics of JEBAR from diagnostic models due to the model inherent errors. The application of JEBAR in the analysis of the ocean circulation still remains controversial (Cane et al. 1998). To better understand the combined effect of baroclinic process and bottom topography, a dynamic, rather than diagnostic, study is necessary. One example is the work of Sakamoto and Yamagata (1996), who investigated the seasonal variation of the Kuroshio transport in terms of JEBAR in a two-layer planetary geostrophic model. But so far, the dynamic studies are still relatively less extensive than the diagnostic studies.

Using a simple model, our focus is to understand the physical mechanism of the joint effect of buoyancy and the continental slope on transport of the western boundary current. Similar to the dynamic study of Simons (1979), we adopt an idealized two-layer quasigeostrophic (QG) model, in which the buoyancy flux is incorporated as a prescribed vertical interfacial mass flux. The joint effect of buoyancy and continental slope is first analyzed in light of Sverdrup dynamics and further verified in numerical model simulations. The paper is organized as the follows. A description of the model is provided in section 2. Model results are provided in section 3. Sensitivity studies are provided in section 4. The conclusions and discussion are presented in section 5.

2. Model formulation

a. The model

We adopt a two-layer QG model with bottom topography $h_b(x, y)$ and a vertical interfacial mass flux $w_s(x, y)$ to parameterize the buoyancy flux (Fig. 1 ). The basic equations are

$$\begin{aligned} \partial_t q_1 + J(\varphi_1, q_1) &= \frac{f_0}{H_1}(w_e - w_s) - A\nabla^6 \varphi_1 \\ \partial_t q_2 + J(\varphi_2, q_2) &= \frac{f_0}{H_2}w_s - A\nabla^6 \varphi_2 - \sigma\nabla^2 \varphi_2, \quad (1) \end{aligned}$$

in which w_e is the Ekman pumping and A and σ are the biharmonic diffusion and bottom friction coefficients, respectively. The upper and lower layer potential vorticity are, respectively,

$$\begin{aligned} q_1 &= \nabla^2 \varphi_1 + \beta y + \frac{f_0^2}{g'H_1}(\varphi_2 - \varphi_1) \\ q_2 &= \nabla^2 \varphi_2 + \beta y + \frac{f_0^2}{g'H_2}(\varphi_1 - \varphi_2) + \frac{f_0}{H_2}h_b. \end{aligned}$$

In the interior ocean, the steady-state solution satisfies

$$\begin{cases} \beta\varphi_{1x} = \frac{f_0}{H_1}(w_e - w_s) & (2a) \\ \beta\varphi_{2x} = \frac{f_0}{H_2}(w_s - w_b), & (2b) \end{cases}$$

where $w_b = J(\Phi_2, h_b)$ is the vertical velocity at the bottom.

The following nondimensional variables are introduced:

$$\begin{aligned} \varphi^* &= \frac{\varphi}{\Psi}; & \delta &= \frac{H_1}{H}; & h_b^* &= \frac{h_b}{H}; \\ (x^*, y^*) &= \frac{1}{L}(x, y); & (w_e^*, w_s^*) &= \frac{1}{W_e}(w_e, w_s); \\ \Psi &= \frac{fW_eL}{\beta H}. \end{aligned}$$

[Equations \(2a,b\)](#) become

$$\begin{cases} \varphi_{1x} = \frac{1}{\delta}(w_e - w_s) \\ \varphi_{2x} = \frac{1}{1 - \delta}(w_s - w_b), \end{cases}$$

where $w_b = \epsilon J(\Phi_2, h_b)$; $\epsilon = f_0/\beta L$. The asterisk that denotes the nondimensional variable has been dropped. The barotropic streamfunction Φ_B can be immediately written as

$$\Phi_{Bx} = \delta\varphi_{1x} + (1 - \delta)\varphi_{2x} = w_e - w_b. \quad (3)$$

The topographic vortex stretching w_b due to the bottom flow can be further rewritten as

$$w_b = \epsilon J(\varphi_2, h_b) = \frac{\epsilon}{1 - \delta} J(\varphi_B, h_b) - \frac{\epsilon\delta}{1 - \delta} J(\varphi_1, h_b). \quad (4)$$

The first term of the right side of [Eq. \(4\)](#) is the barotropic topographic vortex stretching. The second term, traditionally named as the JEBAR term ([Mertz and Wright 1992](#)), is the topographic vortex stretching due to the barotropic flow referenced to the bottom. Substituting the above relation, [Eq. \(4\)](#), into [Eq. \(3\)](#) we have

$$\varphi_{Bx} + \frac{\epsilon}{1 - \delta} J(\varphi_B, h_b) = w_e + \frac{\epsilon\delta}{1 - \delta} J(\varphi_1, h_b). \quad (5)$$

In this formulation, the JEBAR term seems to act as Ekman pumping, which is able to generate a barotropic flow. However, the physical meaning remains unclear. Indeed, if the bottom water is motionless [$w_b = \epsilon J(\Phi_2, h_b) = 0$], the bottom topography has no dynamic effects on the barotropic transport, even though the JEBAR term is nonzero. Thus, it is the *bottom flow* that gives rise to topographic vortex stretching, resulting in an extra barotropic component [see [Eq. \(3\)](#)]. This will be the clue to understanding the joint effect of the baroclin process and topography. For simplicity, only the continental slopes (northern, western, and eastern) with uniform slope and moderate height, within the limits of QG

approximation, are considered here. Other model parameters can be found in [Table 1](#).

b. Buoyancy flux prescription

In our layered model, a cross-interface mass flux will be used to simulate the buoyancy forcing that drives the deep circulation in the ocean. This type of parameterization of cross-interface mass flux can be traced to the classic work by [Stommel and Arons \(1960\)](#) that used an uniform upwelling everywhere. This parameterization has been extended in many directions. A nonuniform upwelling velocity, proportional to the deviation from a constant reference level, was introduced by [Kawase \(1987\)](#). A more recent study of deep-water upwelling can be seen in the paper by [Huang and Yang \(1996\)](#).

In the North Atlantic, both observations and numerical models show that the meridional overturning cell has a narrower region of intense mass sinking at high latitudes and broad compensating upwelling in the midlatitude and equatorial region. For our model study, to approximate the meridional structure of the overturning cell, we make the following distribution:

$$w_s = \theta \{1 - \exp[\mu(y - y_0)]\} \sin(\pi y), \quad (6a)$$

which is assumed to be uniform in the zonal direction. Mass conservation requires

$$Q = \frac{1}{\epsilon} \int_0^{L_x} \int_0^{y_0} w_s dx dy = \frac{1}{\epsilon} \int_0^{L_x} \int_{y_0}^{L_y} |w_s| dx dy, \quad (6b)$$

where Q is the total cross-interface water mass, normalized by the horizontal transport H^{int} ; y_0 separates the narrower downwelling at high latitudes from the broad upwelling in the south. Given Q and y_0 , μ and θ in [Eq. \(6a\)](#) can be uniquely determined from the mass conservation equation.

In choosing Q and y_0 , we have kept in mind the North Atlantic. The wind-driven transport in the subtropic gyre of the North Atlantic is about 40 Sv ($\text{Sv} \equiv 10^6 \text{ m}^3 \text{ s}^{-1}$) and the total deep-water production is about 10~16 Sv, mostly localized in a high-latitude band. So, in the model, Q is set to 1/4 and y_0 to 0.8. [Figure 1](#) plots the meridional distribution of the cross-interface mass flux. Obviously, for a fixed amount of deep-water production, a narrower band will require a faster vertical speed.

3. Mechanism of the joint effect

To highlight the physics of the joint effect of buoyancy and continental slope, we start with a simple case: a northern continental slope in the absence of wind. In this case, the flow in each layer can be obtained analytically. In turn, the JEBAR term can be explicitly expressed in terms of buoyancy flux and continental slope.

a. Northern continental slope: A reduction effect

We adopt the following slope:

$$h_b(x, y) = \begin{cases} s(y - y_b), & y_b \leq y \leq L_y \\ 0, & \text{otherwise} \end{cases}$$

in which s is the slope and y_b is the southern edge of the slope.

The streamfunction in each layer satisfies

$$\begin{cases} \varphi_{1x} = -\frac{1}{\delta} w_s \\ (1 + p)\varphi_{2x} = \frac{1}{1 - \delta} w_s \end{cases} \quad (7)$$

where $p = \epsilon s / (1 - \delta)$ is proportional to the continental slope. Thus, the barotropic transport becomes

$$\varphi_{Bx} = -w_b = -\epsilon J(\varphi_2, h_b) = -\epsilon s \varphi_{2x} = -\frac{p w_s}{1 + p}, \quad (8)$$

which explicitly shows the coupling effect of the buoyancy flux (w_s) and bottom topography (p) on the generation of barotropic flow. Physically, this coupling effect can be understood as follows: in the absence of bottom topography ($p = 0$), the transports driven by the buoyancy flux in the upper and lower layer are of the same magnitudes but opposite directions, resulting in a zero net flow. However, with a northern shoaling continental slope, the mean PV gradient in the lower layer is increased because the bottom topographic β and the planetary β are of the same sign. Thus, the lower flow is reduced. The upper flow, however, remains unchanged because there is no mechanism for this flow to feel bottom topography. As a result, the lower flow can no longer compensate its overlying flow, resulting in a net flow dominated by the upper flow.

It is immediately seen that a steeper continental slope can result in a stronger barotropic flow. This is because a sharper slope will enhance the bottom topographic–beta effect, which will cause a substantial reduction of the deep flow. Similarly, a shallower deep layer (larger δ , therefore larger p) can also intensify the barotropic flow.

Next, wind forcing is turned on by adding Ekman pumping at the top. In the steady state, this effect is trapped in the upper layer. The total barotropic flow is a linear combination of the upper wind-driven flow and the flow generated by buoyancy and topography. In the context of JEBAR formulation, we decompose the total transport into the wind-driven and JEBAR-driven components:

$$\varphi_B = \varphi^{\text{wind}} + \varphi^{\text{JEBAR}},$$

which satisfies

$$\begin{cases} \varphi_x^{\text{wind}} + J(\varphi^{\text{wind}}, h_b) = w_e \\ \varphi_x^{\text{JEBAR}} + J(\varphi^{\text{JEBAR}}, h_b) = \epsilon \delta J(\varphi_1, h_b) / (1 - \delta). \end{cases} \quad (9)$$

Both components can be analytically obtained by

$$\begin{cases} \varphi_x^{\text{wind}} = \frac{w_e}{1 + p} \\ \varphi_x^{\text{JEBAR}} = \frac{p}{1 + p} (w_e - w_s). \end{cases} \quad (10)$$

The ratio of these two components is

$$r = \frac{\varphi_x^{\text{JEBAR}}}{\varphi_x^{\text{wind}}} = p \left(1 - \frac{w_s}{w_e} \right). \quad (11)$$

So, in ocean regions where the buoyancy forcing dominates, the horizontal transport is mainly determined by the JEBAR. An occurrence of this relationship is implied in the North Atlantic subpolar region where strong buoyancy forcing and a northern continental slope exist. Diagnostic studies clearly show that excluding the JEBAR term in the Irminger Sea can lead to a significant reduction, or even the disappearance, of the subpolar gyre, as previously studied in more realistic cases ([Greatbatch et al. 1991](#); [Myers et al. 1996](#)).

It should be noted that, even in the absence of buoyancy flux ($w_s = 0$), the transport driven by JEBAR is still considerable. However, this does not give any additional component to the total transport, which is just the upper-layer transport driven by Ekman pumping. In this sense, one should be careful to interpret the diagnostic calculation in terms of the JEBAR formulation.

b. Western continental slope: A deflection effect

In this case, the continental slope is prescribed as

$$h_b(x, y) = \begin{cases} s(x_b - x), & 0 \leq x \leq x_b \\ 0, & \text{otherwise.} \end{cases}$$

Over the continental slope, the lower-layer streamfunction becomes


$$\varphi_{2x} + p\varphi_{2y} = \frac{w_s}{1 - \delta}, \quad (12)$$


which can be solved by the characteristic method. The corresponding characteristic equations are

$$\frac{dx}{ds} = 1; \quad \frac{dy}{ds} = p; \quad \frac{d\varphi_2}{ds} = \frac{w_s}{1 - \delta}. \quad (13)$$

The upper-layer flow, however, remains the same as that in the case of no topography.

1) PURE BUOYANCY-DRIVEN FLOW


First, we isolate the effect of buoyancy forcing by turning off the wind forcing ($w_e = 0$). Typical flow patterns in the upper and lower layers are illustrated in [Figs. 2a and 2b](#) , which plot the transports $\delta\varphi_1$ and $(1 - \delta)\varphi_2$. In the upper layer, the flow is purely driven by the buoyancy flux, with a narrower intense cyclonic gyre in the north due to the vortex stretching ($w_s < 0$) and a broader anticyclonic gyre in the south due to the vortex compression ($w_s > 0$). Both gyres are not closed at the western boundary region due to the absence of damping in the model. The deep circulation is much different from the upper circulation and can be separated into three regions. In region A, where the bottom is flat, the flow is just a reversal of the upper flow, with vortex compression in the north ($w_s < 0$) and vortex stretching in the south ($w_s > 0$). In region B, the flow is significantly distorted by the continental slope. As the westward flow of region A reaches the edge of the continental slope, the flow must turn southwestward to satisfy potential vorticity conservation by reducing its planetary vorticity. As a result, water from the high latitudes of the region A is completely blocked to south of geostrophic contour P. Consequently, in the northwestern corner (region C), the flow is much weaker than its counter part in the upper layer, where the flow has a long acceleration path.

Due to the deflection effect of the western continental slope, the flow in the deep layer can no longer compensate the overlying upper-layer flow as it did in the flat-bottom region. This situation is clearly shown by the barotropic transport plotted in [Fig. 2c](#) . The typical pattern is a cyclonic gyre, confined in the northwestern corner and dominated by the upper flow, and an adjacent anticyclonic gyre dominated by the deep flow. A strong jet along geostrophic contour P is formed. In addition, a weak cyclonic gyre, dominated by the lower flow, can be seen in the southwestern corner.

The generation of barotropic flow can also be understood in terms of the bottom vertical velocity, as in the [Holland \(1973\)](#) GCM study. The southwestern flow over the continental slope can generate a positive bottom vertical velocity $w_b = u_2 \partial_x h_b > 0$, thus resulting in a depth-averaged (barotropic) anticyclonic circulation, which is mainly determined by $\varphi_x^B = -fw_b/\beta$.

Results from the analytic model are also compared with the numerical model having stratification and biharmonic eddy mixing ([Schmitz and Holland 1986](#)). To reduce the effect of nonlinear advection (usually ignored in JEBAR discussion), the magnitude of the buoyancy flux is reduced to one percent of its value in the analytic model. Other parameters are the same as in the analytical model. The patterns are quite similar except in the western and southern boundary region where intense boundary currents have been formed to close the gyres (not shown).

c. Combined wind and buoyancy-driven flow

In this case, an antisymmetric Ekman pumping is added. In the upper layer, the common antisymmetric double gyre has been distorted by the buoyancy flux, even though the total amount of cross-interface water mass is only a quarter of the wind-driven mass transport. A significant distortion can be seen in the barotropic flow ([Fig. 2d](#) ). In the eastern region without topography, the buoyancy flux has no contribution to the barotropic flow; thus the flow is purely wind driven. Over the continental slope, the buoyancy flux dramatically intensifies both the subtropic and subpolar gyres. The center of the subtropic gyre has shifted toward the north, causing the midlatitude jet to intrude into the subpolar gyre. A similar feature is also observed in the numerical model (not shown), where an intensified western boundary current overshoots toward the subpolar gyre.

The pattern in our model resembles that in [Holland's \(1973\)](#) GCM study in which an intensified wormlike anticyclonic gyre is observed to occupy the whole western boundary region, extending to the interior with a lobe of wind-driven circulation. The main difference occurs in the northwestern corner, where a cyclonic gyre, appearing in our model, is not shown in the GCM simulation. This difference may be caused by our simplified parameterization of the buoyancy flux, which assumes zonal uniformity.

d. Eastern continental slope: A remote effect

In this case, an eastern continental slope with the same height and zonal extent as the above western continental slope is included. In the eastern region of the lower layer, the westward flow must deflect to the north to conserve its potential vorticity through increased planetary vorticity. Therefore, in the northeastern corner an anticyclonic recirculation is developed. The flow in the western region is also modulated due to the distortion of the incoming flow. Consequently, over the entire basin the deep flow can no longer compensate its overlying flow, thus generating a barotropic transport. Compared with the western continental slope, the barotropic transport resulting from an eastern continental slope is much weaker, both in the subpolar gyre and the subtropic gyre.

4. Sensitivity study

In the section above, the mechanism for generating barotropic flow by the buoyancy flux and continental slope is discussed. In this section, the sensitivity of the joint effect to the model parameters will be studied. We focus on the effects of continental slope geometry. For practical interest, only the western continental slope is considered here, keying on two important configuration parameters: the slope's zonal extent and maximum height.

We start with a simplified form of the interfacial mass flux:

$$w_s = \theta \{1 - \exp[\mu(y - y_0)]\} \sin(\pi y) D(x - x_e) = G(y) D(x - x_e), (14)$$

where D is the Dirichlet kernel, indicating that buoyancy flux only occurs on the eastern boundary. The parameters θ , μ , y_0 , and Q are the same values as those used for the zonally uniform forcing.

In the upper layer, the streamfunction can be easily obtained as

$$\begin{aligned} \varphi_1 &= \left(w_e(y)(x - x_e) - G(y) \int_{x_e}^x D(x - x_e) dx \right) / \delta \\ &= [w_e(y)(x - x_e) + G(y)] / \delta. \end{aligned} \quad (15)$$

In the lower layer, according to the previous discussion, the flow can be separated into three regions. In region A (flat bottom), the streamfunction is

$$\begin{aligned} \varphi_2^A(x, y) &= \frac{1}{1 - \delta} G(y) \int_{x_e}^x D(x - x_e) dx \\ &= -G(y)/(1 - \delta). \end{aligned} \quad (16)$$

In region B (south of the geostrophic contour P), the streamfunction is conservative along a characteristic line. So the solution can be determined in terms of the value on the edge of the continental slope:

$$\varphi_2^B(x, y) = \varphi_2^A(x_b, y_s) = -G(y_s)/(1 - \delta), (17)$$

where

$$y_s = p(x_b - x) + y = \frac{\epsilon h_b}{1 - \delta} \left(1 - \frac{x}{x_b} \right) + y.$$

In region C, all the characteristic lines originate from the northern boundary where the streamfunction is zero. Therefore, no flow exists in that domain.

We focus on region B where the barotropic streamfunction can be explicitly expressed as

$$\Psi_B = \delta\Psi_1 + (1 - \delta)\Psi_2 = [w_e(y)(x - x_e) + G(y)] - G(y_s). \quad (18)$$

For the subtropic gyre, if $G(y_s)$ is negative, which means the deep subpolar water can enter into the subtropic region, the barotropic transport of the subtropic gyre will be intensified. It can be seen that an increase in the height or zonal extent of a continental slope can increase the value of y_s , thus intensifying the barotropic transport of the subtropic gyre. The physical mechanism is that an increase in the height or zonal extent of a western continental slope will enhance the southward deflection effect for the subpolar gyre, thus allowing more deep subpolar water to enter into the subtropic gyre. The schematic picture is shown in [Fig. 3](#). In the following, we will quantify the effects of these two parameters when zonally uniform buoyancy forcing is imposed.

a. Effect of the zonal extent of continental slope

In this set of experiments, the topography height is fixed at 1000 m. The zonal extent of the continent slope is increased toward the eastern boundary. The change of the maximum barotropic transport of the subtropic gyre is illustrated in [Fig. 4](#) (the solid curve), which shows a monotonically decreasing trend as the bottom topography changes from a steep continental slope to a gentle continental rise. This tendency is opposite to that found for the case of buoyancy localized on the eastern boundary. Since in the steady state, the bottom topography has no effect on the upper flow, the change of barotropic transport mainly comes from changes to the deep subpolar gyre. For the case of zonally uniform buoyancy flux, a continental slope allows for a longer acceleration path than a continental rise before the deep subpolar water column interacts with the topography. The resulting difference in transport can overwhelm the difference caused by the deflection effect between a continental slope and a rise. Therefore, a continental slope can enhance the incoming flow of the western boundary current in the subtropic gyre.

To test the robustness of the analytic model, we also performed numerical model calculations with the same parameters as in the analytic model except for the inclusion of eddy mixing and stratification. The barotropic transport of the subtropic gyre shows the same tendencies as that in the analytic model except for cases with very steep continental slopes. The numerical model shows that, as the zonal extent of the continental slope becomes smaller than 0.2 (800 km, 20% of the basin zonal size), the transport will eventually decrease, which is opposite to that predicted by the analytic model.

The discrepancy between the analytic and numerical models can be understood in terms of the deep circulation. [Figure 5](#) displays the circulation in the deep layer at $x_b = 0.4$ and 0.1. It can be seen that, as the continental slope becomes much steeper, the water in the center of the deep subpolar gyre, where the flow has a weaker zonal speed ($u \propto \partial_y w_s$), will be blocked at the edge of the slope. Therefore, the western boundary current receives less water from the deep subpolar gyre. In the limit, as the extent of the continental slope approaches zero, the continental slope becomes a vertical wall, completely blocking the subpolar water and eliminating all deflection effects. The transport returns to the wind-driven transport.

b. Effect of the height of continental slope

In this case, the zonal extent of the continental slope is fixed at 0.25 (1000 km, 25% of the basin zonal size). The maximum height of the continental slope increases from 0 to 2000 m. We focus on the transport of the western boundary current.

The change of the barotropic transport as predicted by the analytic model is illustrated in [Fig. 6](#). It can be seen that an increase in the maximum height of the continental slope will enhance the barotropic transport of the subtropic gyre. At $h_b = 0.4$ (1600 m), the transport reaches a maximum value of 3.7 (normalized by the interior Sverdrup transport). Further increase in the continent slope height will slightly reduce the transport.

The effect can be understood in this way. As the continental slope height increases, the deflection effect becomes stronger, permitting the deep flow from subpolar region to enter the subtropic region, thus intensifying the barotropic flow there. Once the center of the deep subpolar gyre overlaps with the center of the upper subtropic gyre, the barotropic transport reaches its maximum value. This correlation gives an estimate for the peak transport to occur at $h_b = 0.41$, which is very close to the model result. Further increases in the continental slope height will deflect the center of the deep subpolar gyre south of the upper subtropic gyre center, slightly reducing the barotropic transport of the western boundary current.

The results calculated by the numerical model are also shown in [Fig. 4](#) (marked by circles). The tendency of the barotropic transport when h_b is smaller and the height of the continental slope where the peak transport occurs are very similar to the analytic model result. However, as the continental slope becomes steeper ($h_b > 0.4$), the water in the center of the deep subpolar gyre is unable to enter the subtropic region due to the same mechanism discussed in the previous section. Therefore, the transport of the subtropical gyre is reduced.

It should be pointed out that, for a very steep continental slope, the finite topography effect omitted in the current QG model may affect the dynamics of ocean circulation. To further test the robustness of our analytical model results, we performed several additional experiments using a primitive equation layered model ([Wallcraft 1991](#)) with the same parameters as used in our QG model. While small quantitative differences exist, the tendency of the barotropic transport and the height of continental slope where the barotropic transport peaks are consistent with those found in the QG model.

5. Summary and discussion

In this paper, the dynamics of the joint effect of buoyancy and continental slope on ocean circulation is studied using a two-layer quasigeostrophic model. In the model, buoyancy is incorporated as an interfacial mass flux, having narrow intense detrainment in the high latitudes and broad weak entrainment elsewhere.

The model immediately shows that, in the presence of the bottom topography, a small amount of buoyancy flux can generate a strong barotropic flow. Because the bottom topographic–beta effect modulates the buoyancy-driven deep flow, preventing compensation of the overlying buoyancy-driven flow, net transport is generated. Specifically, with a northern continental slope, the topographic–beta effect *reduces* the deep buoyancy-driven flow, producing a barotropic flow where the upper flow dominates. With a western continental slope, the topographic–beta effect *deflects* the deep flow toward the southwest so that it is no longer overlapped by its upper-layer counterpart. With an eastern continental slope, the deep flow in the western region is *remotely* modulated by the bottom topography, due to the northwestern deflection of its incoming flow.

In a double gyre circulation, the model shows that, in the presence of a western continental slope, a small amount of interfacial mass flux can significantly intensify the western boundary current transport. The sensitivity studies demonstrate that an increase in the height of the continental slope can enhance the barotropic transport. This comes from the fact that an increase of the continental slope height can deflect the deep subpolar flow into the deep subtropic region, thus intensifying the inflow to the western boundary current. The model also shows differences between a continental slope and a continental rise. With a steep continental slope, the water in the center of the deep subpolar gyre is blocked at the edge of the slope and, therefore, less water can enter to the subtropic region to intensify the barotropic flow there.

This model can help with understanding the physical mechanism of the coupling effect of buoyancy and the continental slope on the western boundary current and, also, produce a satisfactory quantitative estimate on the Gulf Stream transport. For a basin 4000 km square with a moderate western continental slope ($x_b = 1000$ km, $h_b = 1600$ m), if 10 Sv water sinks from the upper layer to deep layer, the western boundary current transport can be increased from 40 Sv of the wind-driven transport to 148 Sv.

It should be pointed out that, in all of the discussions about the joint effect of baroclinicity and bottom topography, nonlinear advection has always been ignored. In reality, however, the nonlinear advection may have strong interaction with bottom topography and buoyancy. In a study of the continental slope effect on ocean circulation, [Thompson \(1995\)](#) showed that, even in the absence of buoyancy flux, the continental slope can significantly distort the antisymmetric double gyre circulation. This is because, in the midlatitudes, the nonlinear advection gives rise to recirculations, which can extend to the deep bottom topography, thus generating a bottom velocity ([Liu 1990](#); [Özgekmen et al. 1997](#)).

To illustrate the interaction of buoyancy forcing, bottom topography, and inertia, four additional experiments were performed using the above eddy-resolving QG model. Experiment I is the control run, which is solely driven by the wind. Experiment II was designed to study the effect of the continental slope on the western boundary current transport, where the buoyancy flux has been turned off. Experiment III was designed to study the buoyancy effect without bottom topography. Experiment IV includes all three components: buoyancy forcing, bottom topography, and inertia. From the previous zonal extent sensitivity experiments, we pick the continental slope over which the western boundary current achieves its maximum transport (2.5 times the interior Sverdrup transport). Except for the magnitudes of the Ekman pumping and interfacial mass flux, all the other model parameters including the ratio Q of the two forcings are the same as in the previous linear analysis. In the experiments, the magnitude of the wind-driven transport is 30 Sv and the total water mass sinking from the upper layer to the deep layer is 7.5 Sv. The linear model predicts that the transport of the western boundary current can be increased to 75 Sv.

The barotropic transports (normalized by the interior Sverdrup transport) for these four experiments are shown in [Fig. 7](#). In the control case, the antisymmetric *wind curl* drives two recirculations that flank the midlatitude jet, which in turn substantially intensifies the transport of the western boundary current ([Fig. 7a](#)). The model shows the transport of the western boundary current increases well above that found from the Sverdrup balance of 30 Sv to 120 Sv. When the continental slope is included, away from the western boundary the transport distribution is similar to the flat-bottom experiment ([Fig. 7b](#)). Near the western boundary, the symmetry of the double gyres is destroyed. After leaving the coast, the western boundary current must shift northward to overcome the potential vorticity deficit caused by the eastward deepening of continental slope, thus developing a meandering midlatitude jet. Consequently, the zonal recirculation gyres are affected and the maximum transport is reduced to 72 Sv in the subtropic gyre and 75 Sv in the subpolar gyre. In this case, the influence of the continental slope on the western boundary current is activated by the vertical extension of the recirculation gyres, which are driven by the nonlinear advection of vorticity. This nonlinear vorticity advection can also enhance the influence of baroclin buoyancy-driven flow on the barotropic transport of the western boundary current, even in the absence of the bottom topography. When buoyancy is included ([Fig. 7c](#)), in the region away from the western boundary, the buoyancy flux has no effect on barotropic flow. The flow pattern is the same as the wind-driven pattern. Near the western boundary, however, there are major differences. The western boundary current overshoots toward the north, and the midlatitude zonal jet is deflected to the north of the zero wind curl line. While the strength of recirculation in the subtropical gyre remains almost the same as in the control case, the maximum transport of the subpolar gyre is increased to 165 Sv. This change is associated with strong detrainment in the high latitudes, which dramatically intensifies the incoming flow of the subpolar western boundary current in the upper layer, thereby accelerating the vorticity advection toward the midlatitude and producing a strong recirculation. Near the northern boundary there is a gyre, which is not shown in the linear model. This is the subpolar recirculation gyre driven by the buoyancy in the deep layer. Furthermore, when the continental slope is included ([Fig. 7d](#)), the buoyancy enhances the incoming flow of the subtropical western boundary current through the deflection effect of the continental slope, as discussed in the linear model study. Therefore, the subtropical recirculation gyre is substantially intensified and the maximum barotropic transport is increased to 140 Sv, 4.7 times the wind-driven Sverdrup transport and well above that predicted by the linear model (75 Sv). In contrast, the recirculation gyre in the subpolar gyre is reduced to 78 Sv. The overall pattern resembles that found by the linear calculations.

In short, in the presence of inertia, either buoyancy forcing or the continental slope alone can substantially affect the western boundary current. The continental slope tends to reduce the transport of the western boundary current, and buoyancy forcing tends to enhance the subpolar recirculation gyre and push the western boundary current to overshoot. However, when both buoyancy forcing and continental slope are included, the deflection effect of the continental slope on the deep subpolar gyre can enhance the inertial effect, thus intensifying the transport of the western boundary current.

In terms of the coupling effect between the continental slope and buoyancy, our simple idealized model can shed a little light on understanding the difference in transports between the Gulf Stream and Kuroshio Current. In the presence of bottom topography, the stronger buoyancy flux in the North Atlantic, versus that in the North Pacific, favors greater transport for the Gulf Stream. Recent comprehensive diagnostic studies of the North Atlantic have shown that, if the JEBAR term were excluded in the region between 30° and 40°N, 50° and 70°W where significant topographic variation exists ([Greatbatch et al. 1991](#); [Myers et al. 1996](#)), the strength of the Gulf Stream would be dramatically reduced. A high-resolution model of the North Atlantic clearly shows that, in that region, the North Atlantic Deep Water flow has a southwestward tendency, eventually attaching to the western boundary to form a coherent boundary current at 35°N ([Bryan et al. 1995](#)). This southwestward flow could give rise to a positive bottom vertical velocity, which would intensify the Gulf Stream where the westward shoaling topography dominates. Direct application of our model is severely limited by the chosen implementation of buoyancy forcing, which is simply prescribed everywhere. Future work will use a more generic parameterization including the zonal variation, especially in the region of the western boundary current. This will be our next focus.

Acknowledgments

We would like to thank Dr. T. Yamagata for a discussion that strongly motivated this work and two anonymous reviewers for their constructive comments. We also thank Mr. Eric Bayler for editorial help. This work is supported by the Young Investigator Award/ONR and the Physical Oceanography Program/NSF.

REFERENCES

- Bryan, F. O., C. W. Böning, and W. R. Holland, 1995: On the midlatitude circulation in a high-resolution of the North Atlantic. *J. Phys. Oceanogr.*, **25**, 289–305.. [Find this article online](#)
- Cane, M. A., V. M. Kamenkovich, and A. Krupitsky, 1998: On the utility and disutility of JEBAR. *J. Phys. Oceanogr.*, **28**, 519–526.. [Find this article online](#)

- Greatbatch, R. J., A. F. Fanning, A. D. Goulding, and S. Levitus, 1991: A diagnosis of interpentadal circulation changes in the North Atlantic. *J. Geophys. Res.*, **96**, 22 009–22 023..
- Holland, W. R., 1973: Baroclinic and topographic influences on the transport in western boundary currents. *Geophys. Fluid Dyn.*, **4**, 187–210..
- Huang, R. X., and J. Yang, 1996: Deep-water upwelling in the frictional western boundary current. *J. Phys. Oceanogr.*, **26**, 2243–2250.. [Find this article online](#)
- Hurlburt, H. E., A. J. Wallcraft, W. J. Schmitz, P. J. Hogan, and E. J. Metzger, 1996: Dynamics of Kurishio/Oyashio current system using eddy-resolving models of the North Pacific Ocean. *J. Geophys. Res.*, **101**, 941–976..
- Huthnance, J. M., 1984: Slope currents and “JEBAR.” *J. Phys. Oceanogr.*, **14**, 795–810.. [Find this article online](#)
- Kawase, M., 1987: Establishment of deep ocean circulation driven by deep-water production. *J. Phys. Oceanogr.*, **17**, 2294–2317.. [Find this article online](#)
- Joyce, T. M., and W. J. Schmitz, 1988: Zonal velocity structure and transport in the Kurishio Extension. *J. Phys. Oceanogr.*, **18**, 1484–1494.. [Find this article online](#)
- Liu, Z., 1990: On the influence of the continental slope on the western boundary layer: The enhanced transport and recirculation. *J. Mar. Res.*, **48**, 255–185..
- Mellor, G. L., C. R. Mechoso, and E. Keto, 1982: A diagnostic calculation of the general circulation of the Atlantic Ocean. *Deep-Sea Res.*, **29**, 1171–1192..
- Mertz, G., and G. D. Wright, 1992: Interpretations of the JEBAR term. *J. Phys. Oceanogr.*, **22**, 301–305.. [Find this article online](#)
- Myers, P. G., A. F. Fanning, and A. J. Weaver, 1996: JEBAR, bottom pressure torque, and Gulf Stream. *J. Phys. Oceanogr.*, **26**, 671–683.. [Find this article online](#)
- Özgokmen, T. M., E. P. Chassignet, and A. M. Paviva, 1997: Impact of wind forcing, bottom topography, and inertia on midlatitude jet separation in a quasigeostrophic model. *J. Phys. Oceanogr.*, **27**, 2460–2476.. [Find this article online](#)
- Sakamoto, T., and T. Yamagata, 1996: Seasonal transport variations of the wind-driven ocean circulation in a two-layer planetary geostrophic model with a continental slope. *J. Mar. Res.*, **54**, 261–284..
- Sarkisyan, A. S., and V. F. Ivanov, 1971: Joint effect of baroclinicity and bottom relief as an important factor in the dynamics of sea current. *Izv. Acad. Sci. USSR Atmos. Oceanic Phys.* (English trans.), **7**, 173–188..
- Schmitz, W. J., Jr., and W. R. Holland, 1986: Observed and modeled mesoscale variability near the Gulf Stream and Kuroshio extension. *J. Geophys. Res.*, **91**, 9624–9638..
- , and M. S. McCartney, 1993: On the North Atlantic circulation. *Rev. Geophys.*, **31**, 29–49..
- Simons, T. J., 1979: On the joint effect of baroclinicity and topography. *J. Phys. Oceanogr.*, **9**, 1283–1287.. [Find this article online](#)
- Stommel, H., and A. B. Arons, 1960: On the abyssal circulation of the world ocean I. Stationary planetary flow pattern on a sphere. *Deep-Sea Res.*, **6**, 140–154..
- Thompson, L., 1995: The effect of continental rises on the wind-driven ocean circulation. *J. Phys. Oceanogr.*, **25**, 1296–1316.. [Find this article online](#)
- Wallcraft, A. J., 1991: The Navy Layered Ocean Model Users Guide. NOARL Rep. 35, Naval Oceanographic and Atmospheric Research Lab., Stennis Space Center, MS, 21 pp..

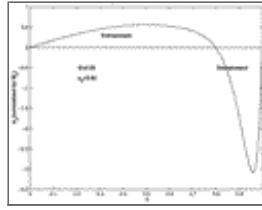
Tables

Table 1. Parameters for the eddy-resolving QG model.

--

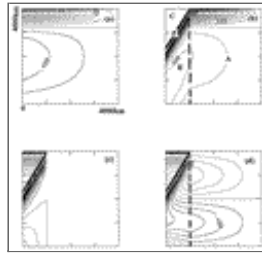
[Click on thumbnail for full-sized image.](#)

Figures



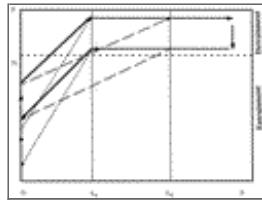
[Click on thumbnail for full-sized image.](#)

Fig. 1. Meridional distribution of the interfacial mass flux w_s normalized by the Ekman pumping velocity. The total mass sinking from the upper layer to lower layer is a quarter (Q) of the wind-driven Sverdrup transport. The sinking region accounts for 20% of the basin.



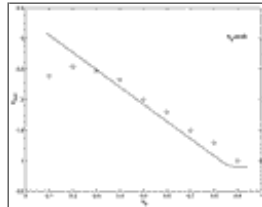
[Click on thumbnail for full-sized image.](#)

Fig. 2. Contour plots of the streamfunction driven by the buoyancy in each layer. The height and zonal extension of continental slope are 1000 m (h_b) and 1000 km (x_b). (a) Upper layer, (b) lower layer, (c) barotropic, and (d) barotropic transport driven by the Ekman pumping and buoyancy. The contour interval in each plot is 0.20 (normalized by the interior Sverdrup transport).



[Click on thumbnail for full-sized image.](#)

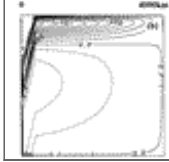
Fig. 3. Schematic plot of the deflection of the deep subpolar gyre by the western continental slope. The solid arrows represent the control case (x_{b1}, h_{b1}). The short-dashed arrows represents the case ($x_{b1}, h_{b2} > h_{b1}$). The long-dashed arrows represent the case ($x_{b2} > x_{b1}, h_{b1}$). Increasing the height and zonal extension of the western continental slope will deflect the subpolar gyre farther toward southwest.



[Click on thumbnail for full-sized image.](#)

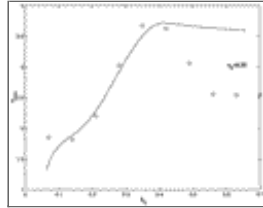
Fig. 4. Change of the maximum transport of the subtropic gyre as the zonal extent of continental slope changes. The maximum height of continental slope is fixed at 1000 m. The transport has been normalized by the interior Sverdrup transport.





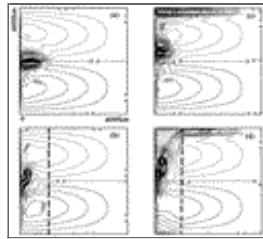
[Click on thumbnail for full-sized image.](#)

Fig. 5. Contour plots of the lower-layer streamfunction for the western continental slope, with (a) $x_b = 1600$ km and (b) 400 km, respectively. The maximum height of continental slope is fixed at 1000 m. The contour interval is 0.20 (normalized by the interior Sverdrup transport).



[Click on thumbnail for full-sized image.](#)

Fig. 6. Change of the maximum transport of the subtropic gyre as the height of the continental slope changes. The zonal extent of the continental slope is fixed at 1000 km. The transport has been normalized by the interior Sverdrup transport.



[Click on thumbnail for full-sized image.](#)

Fig. 7. Contour plots of the barotropic streamfunction (a) flat bottom and wind-driven only, (b) continental slope and wind-driven only, (c) flat bottom, wind- and buoyancy-driven, and (d) continental slope, wind- and buoyancy-driven. The height and zonal extension of continental slope are 1000 m (h_b) and 1000 km (x_b). The wind-driven Sverdrup transport is 30 Sv and the deep-water production is 7.5 Sv. The contour interval is 0.20, corresponding to 6 Sv.

Corresponding author address: Lixin Wu, Department of Atmospheric and Oceanic Science, University of Wisconsin—Madison, 1225 W. Dayton Street, Madison, WI 53706.

E-mail: lxw@ocean.meteor.wisc.edu

[top ▲](#)



© 2008 American Meteorological Society [Privacy Policy and Disclaimer](#)
 Headquarters: 45 Beacon Street Boston, MA 02108-3693
 DC Office: 1120 G Street, NW, Suite 800 Washington DC, 20005-3826
amsinfo@ametsoc.org Phone: 617-227-2425 Fax: 617-742-8718
[Allen Press, Inc.](#) assists in the online publication of AMS journals.